PNAS RESEARCH ARTICLE | DEVELOPMENTAL BIOLOGY

Polycomb group (PcG) proteins prevent the assembly of abnormal synaptonemal complex structures during meiosis

Tália Feijão[a,b,c,1], Bruno Marques[a,1], Rui D. Silva[a,d], Célia Carvalho[e], Daniel Sobral[f,g], Ricardo Matos[a], Tian Tan[h], António Pereira[b], Eurico Morais-de-Sá[b], Hélder Maiato[b], Steven Z. DeLuca[h], and Rui Gonçalo Martinho[a,c,e,2]

Edited by Margaret Fuller, Stanford University School of Medicine, Stanford, CA; received March 16, 2022; accepted July 18, 2022

The synaptonemal complex (SC) is a proteinaceous scaffold that is assembled between paired homologous chromosomes during the onset of meiosis. Timely expression of SC coding genes is essential for SC assembly and successful meiosis. However, SC components have an intrinsic tendency to self-organize into abnormal repetitive structures, which are not assembled between the paired homologs and whose formation is potentially deleterious for meiosis and gametogenesis. This creates an interesting conundrum, where SC genes need to be robustly expressed during meiosis, but their expression must be carefully regulated to prevent the formation of anomalous SC structures. In this manuscript, we show that the Polycomb group protein Sfmbt, the *Drosophila* ortholog of human MBTD1 and L3MBTL2, is required to avoid excessive expression of SC genes during prophase I. Although SC assembly is normal after Sfmbt depletion, SC disassembly is abnormal with the formation of multiple synaptonemal complexes (polycomplexes) within the oocyte. Overexpression of the SC gene *corona* and depletion of other Polycomb group proteins are similarly associated with polycomplex formation during SC disassembly. These polycomplexes are highly dynamic and have a well-defined periodic structure. Further confirming the importance of Sfmbt, germ line depletion of this protein is associated with significant metaphase I defects and a reduction in female fertility. Since transcription of SC genes mostly occurs during early prophase I, our results suggest a role of Sfmbt and other Polycomb group proteins in downregulating the expression of these and other early prophase I genes during later stages of meiosis.

meiosis | transcription | Polycomb group proteins | synaptonemal complex | polycomplexes

Significance

Timely expression of synaptonemal complex (SC) genes is essential for stabilization of homolog pairing, recombination, and accurate segregation of meiotic chromosomes. However, SC components have an intrinsic tendency to self-organize into abnormal repetitive structures. This creates an interesting conundrum, where SC genes need to be robustly expressed during early prophase I, but their expression must be carefully regulated during meiosis. Here, we show that the Polycomb group (PcG) proteins prevent the unrestrained expression of SC genes during mid/late prophase I, which is critical to avoid the formation of polycomplexes during diplotene. Our results highlight the importance of PcG proteins for the correct regulation of gene expression during prophase I.

Female gametogenesis imposes several challenges for gene expression, as meiosis and the genetic programs required for oocyte determination and differentiation are intertwined during oogenesis. Mitotic to meiotic transition is associated with a genome-wide reprogramming of the germ cells transcriptome, which ensures commitment to female gametogenesis, meiosis, and the correct expression of prophase I genes. Budding yeast transcription factor IME-1 is crucial for sporulation and expression of early sporulation-specific genes, and its overexpression is sufficient to induce meiotic entry (1, 2). In mammals, entry into meiosis is associated with retinoic acid signaling and the transcription factor *Stimulated by retinoic acid 8* (*Stra8*) (3, 4). STRA8 is required within the germ cells for mitotic to meiotic transition, and this transcription factor induces the expression of thousands of genes, including meiotic prophase I genes (5, 6). How the expression of prophase I genes is regulated after induction is nonetheless still poorly understood.

We focused on the expression of the synaptonemal complex (SC) genes, as they are robustly expressed during the onset of meiosis (7), for synapsis formation and meiotic recombination. However, their expression must be tightly regulated during prophase I in order to avoid the intrinsic tendency of these proteins to self-organize into abnormal SC structures, which are not assembled between the paired homologs and whose formation is potentially deleterious for meiosis and gametogenesis (8, 9). This suggests an interesting conundrum, where SC genes need to be robustly expressed during early prophase I for correct SC assembly, but their expression must be carefully regulated to avoid the formation of anomalous structures. Supporting this possibility, ectopic expression of yeast SC component Zip1 and precocious translation of *Caenorhabditis elegans* SC genes during the premeiotic mitotic divisions are both associated with the formation of abnormal SC structures during pachytene (10, 11).

Meiotic prophase I progression relies on pairing of the homologous chromosomes, synapsis formation, and correct formation and maturation of meiotic cross-overs (12). The SC is a proteinaceous scaffold that is assembled between the paired homologous chromosomes during meiosis I and is required to stabilize chromosome pairing interactions (13). Regardless of the requirement of programmed double-strand breaks (DSBs)

Author contributions: T.F., B.M., S.Z.D., and R.G.M. designed research; T.F., B.M., R.D.S., C.C., R.M., T.T., A.P., S.Z.D., and R.G.M. performed research; T.F., B.M., R.D.S., C.C., D.S., R.M., T.T., E.M.-d.-S., H.M., S.Z.D., and R.G.M. analyzed data; R.G.M. wrote the paper; T.F., B.M., R.D.S., D.S., E.M.-d.-S., H.M., and S.Z.D. manuscript review and editing; and R.G.M. funding acquisition.

The authors declare no competing interest.

This article is a PNAS Direct Submission.

[1]T.F. and B.M. contributed equally to this work.

[2]To whom correspondence may be addressed. Email: rgmartinho@ua.pt.

This article contains supporting information online at http://www.pnas.org/lookup/suppl/doi:10.1073/pnas.2204701119/-/DCSupplemental.

Published October 10, 2022.

for homolog pairing and SC assembly (14–16), synapsis formation typically results from a zipper-like process that allows the extension of the initial complexes and full assembly of the SC along the length of the paired chromosome arms during pachytene (17). SC assembly is important for accurate segregation of meiotic chromosomes, and mutations within SC component encoding genes have been linked to infertility, miscarriages, and genetic birth defects, highlighting the importance of this protein complex for human health (18).

Drosophila oogenesis starts in the germarium with an asymmetric division of an anteriorly localized germ line stem cell and the formation of a cystoblast daughter cell. The cystoblast then undergoes four rounds of incomplete mitotic divisions to produce a cyst of 16 interconnected cells. Initial pairing of the homologous chromosomes occurs during these premeiotic mitotic divisions, and once the 16-cell cyst is formed, the paired centromeres cluster on average into two groups (19, 20). SC loading to the centromeres is required for normal clustering of the centromeres in 16-cell cysts (13, 19, 20). Initially up to four nuclei within the 16-cell cyst assemble SCs along their euchromatic arms; however, as the cyst matures, the euchromatic SC disassembles from three of these nuclei, and only the single prooocyte maintains a full-length SC in region 3 of the germarium.

Drosophila SC is composed of three components: two lateral elements that run along the chromosomes and are composed of the cohesin-related Orientation disrupter (Ord) and Crossover suppressor on 2 of Manheim [C(2)M] complexes, a central region that is composed primarily of the transverse filament protein Crossover suppressor on 3 of Gowen [C(3)G] and Corolla, and a central element that contains a protein named Corona (Cona) (13, 21–27). Expression of SC genes starts during the premeiotic mitotic divisions of the cyst, as central region proteins can be seen transiently associated with the centromere before entry into meiosis (19). Consistently, it was recently shown using single-cell RNA sequencing (RNA-seq) that SC genes are transiently transcribed within 8- and 16-cell cysts (7). The SC is fully assembled by region 3 of the germarium (pachytene) and stays assembled within the oocyte until stage 5 of oogenesis, after which it will be progressively disassembled from the chromosome arms (diplotene). By stages 7/8, the SC is no longer detectable in the arms. However, the SC can still be detected within the centromeric regions of meiotic chromosomes at least until stages 8/9 (20). Regulation of SC disassembly during diplotene is poorly understood. In *Saccharomyces cerevisiae*, *C. elegans*, and *Mus musculus*, regulation of SC disassembly is related to cell-cycle kinases such as Polo-like kinases, Aurora B/INCENP, and Cdk1 (28–32). In *Drosophila melanogaster*, regulation of SC disassembly is potentially associated with loading of condensin protein complexes (33).

Our working hypothesis is that expression of prophase I genes is dynamically regulated for meiotic progression and correct maturation of the oocyte. Previously, we and others showed that Lysine demethylase 5 (also known in *Drosophila* as little imaginal discs) is important within the female germ line for maintenance of SC assembly, meiotic chromatin architecture, and female fertility (34, 35). We reasoned that distinct chromatin remodeling proteins likely play an important role in regulating prophase I gene expression and avoiding excessive expression of SC components. To identify such proteins, we performed an RNA interference (RNAi) screen for genes whose depletion within the female germ line would impair the normal assembly and disassembly of the SC. We identified the Polycomb repressive protein Scm-related gene containing four mbt domains (*Sfmbt*) (36–38), the *Drosophila* ortholog of human MBTD1 and L3MBTL2, as being essential for correct disassembly of the SC. Depletion of Sfmbt within the female germ line did not impair the normal assembly of the SC during early prophase I (pachytene), with correct clustering of the centromeres. However, during mid/late prophase I (diplotene), Sfmbt depletion was associated with SC disassembly defects and the formation of a complex network of abnormal SC structures named polycomplexes. Our results provide evidence for the formation of polycomplexes in the absence of previous defects in SC assembly, which uncovers a physiological role of this polycomplex-avoidance mechanism in wild-type oocytes.

Transcriptomic analysis and reverse-transcription droplet digital PCR (RT-ddPCR) showed an up-regulation of several SC genes expression after Sfmbt depletion. Consistent with the hypothesis that unrestrained transcription of SC genes is deleterious, overexpression of the SC component Corona was sufficient to partially phenocopy the formation of polycomplexes, and an increase in gene copy number of SC component Corolla enhanced the polycomplexes phenotype after Sfmbt depletion. Sfmbt and its interacting partner Pleiohomeotic (Pho) associate with regulatory sequences near the corona gene, demonstrating that the Pho repressive complex (PhoRC) directly inhibits corona expression. Further confirming the role of Sfmbt as a key player in the epigenetic regulation of prophase I gene expression, its depletion was associated with significant metaphase I defects, abnormal gametogenesis, and female sterility.

Results

Sfmbt Is Required for the Correct Disassembly of the SC. Timely expression of SC components is essential for chromosome pairing, meiotic recombination, and successful meiosis, yet how these genes are coherently transcribed during prophase I progression is still poorly understood. We reasoned that prophase I expression of SC components is likely regulated at the chromatin level. To test this hypothesis, we performed an RNAi screen for chromatin remodeling genes whose germ line depletion could impair SC assembly and/or disassembly. To screen for germ line regulators of SC dynamics, we used an endogenously expressed green fluorescent protein (GFP)–tagged Corolla (39), a component of the central region of the SC, the germ line specific driver nanos-Gal4 (40), and the UAS/Gal4 system (41, 42) for tissue-specific expression of different short hairpin RNAs (shRNAs) against distinct chromatin remodeling proteins. We identified an Scm-related gene containing four mbt domains (*Sfmbt*) (36, 38) as being a key regulator of SC disassembly. In order to avoid off-target effects, two different nonoverlapping shRNAs (Sfmbt RNAi-1 and Sfmbt RNAi-2) were used in this work. Sfmbt RNAi-1 is available at Bloomington *Drosophila* Stock Center (BDSC; BL32473; hairpin reference P; TRiP.HMS00473) (43), whereas Sfmbt RNAi-2 stock was custom-made (for additional information, see *SI Appendix, Materials and Methods*). As negative control, we used a short hairpin against mCherry, a red fluorescent protein derived from a sea anemone and not expressed in *Drosophila*.

Germ line depletion of Sfmbt did not impair the correct assembly of the SC during pachytene, with normal expression of Corolla and C(3)G along the meiotic chromosomes (region 3 of the germarium) (*SI Appendix*, Fig. S1*A*). Correct assembly of the SC is required for centromere clustering (19, 20). Supporting our conclusion that Sfmbt is not critical for SC assembly, centromere clustering was similarly not affected by Sfmbt depletion (*SI Appendix*, Fig. S1*B*; see quantification in SI Appendix, Fig. S1*C*). In contrast, we detected the formation of abnormal Corolla-positive filaments after the onset of SC

disassembly (from stage 5 onward) (Fig. 1*A*, see yellow arrowheads; see quantification in Fig. 1*C*), which did not colocalize with DNA and were mostly formed in later vitellarium stages. Reassuringly, formation of Corolla-positive filaments after Sfmbt depletion could be detected in the absence of the GFP-tagged Corolla reporter transgene (*SI Appendix*, Fig. S2*A*, see yellow arrowheads; see quantification in *SI Appendix*, Fig. S2*B*), which showed that this phenotype is not dependent on this reporter transgene. We therefore concluded that Sfmbt is not essential for the correct assembly of the SC during pachytene, but its function within the germ line is critical for the correct disassembly of the SC during diplotene.

Sfmbt Represses the Formation of Polycomplexes during SC Disassembly. Defects in SC assembly can be associated with the formation of abnormal SC structures during pachytene (9, 44). This phenomenon is conserved from yeast to humans and results from the intrinsic tendency of SC components to self-organize into abnormal structures not associated with the paired homologous chromosomes. Depletion of Sfmbt led to the formation of abnormal Corolla-positive filaments during SC disassembly (diplotene) (Fig. 1*A*). Since these filaments were reminiscent of a particular type of abnormal SC structures named polycomplexes, we decided to investigate the formation and nature of these structures in more detail.

Drosophila SC disassembly along the meiotic chromosome arms starts at stages 4/5 of oogenesis, and the SC is completely dismantled by stages 8/9 (20). After Sfmbt depletion, Corolla-positive filaments were only detected from stage 5 onward (Fig. 1 *A*, *C*, and *D* and *SI Appendix*, Fig. S2 *A* and *B*), which confirmed that their formation correlated with the onset of SC disassembly. Remarkably, the size of such filaments increased

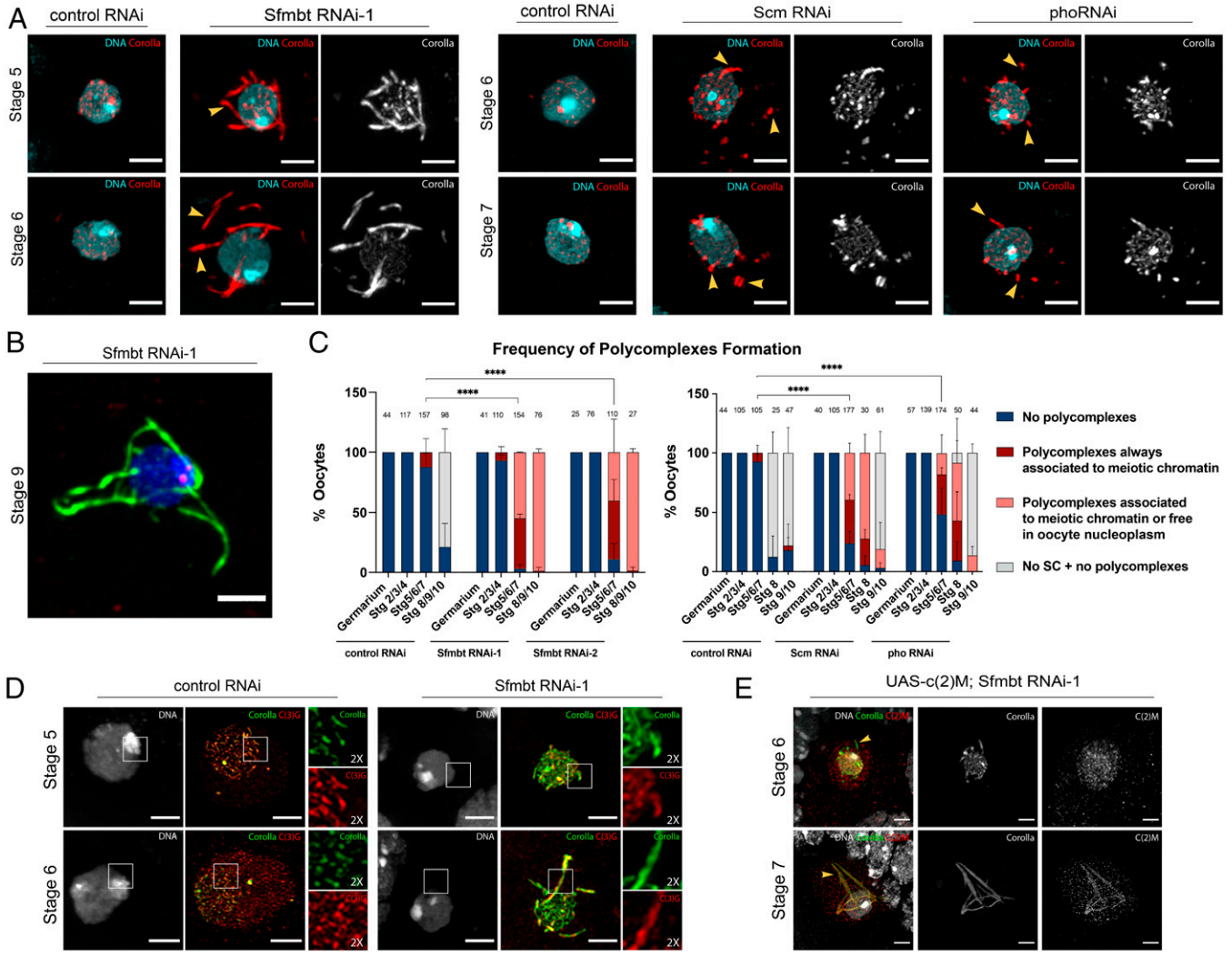

Fig. 1. Sfmbt is required for the correct disassembly of the SC and avoidance of abnormal SC structures (polycomplexes). (*A, B, D*, and *E*) Immunofluorescence images showing the formation of abnormal SC structures (polycomplexes) during midoogenesis (stages 5 to 7) and mid/late oogenesis (stage 9) after germ line depletion of Sfmbt, Scm, and Pho. (*A*) DNA (cyan) and Corolla (Corolla-GFP; red). Arrowheads highlight the polycomplexes in stage 5 to 7 egg chambers. (*B*) DNA (blue), Corolla (Corolla-GFP; green), and Cid (red). Stage 9 egg chamber after germ line depletion of Sfmbt. (*C*) Quantification of polycomplex formation for control RNAi, *Sfmbt*, *Scm*, and *pho* RNAi using an endogenously expressed GFP-tagged Corolla transgene. Number of scored oocytes is displayed on the top of each bar. Statistically significant differences are marked with **** ($P < 0.0001$, Fisher's exact test). Average ± SD of three biological replicas. (*D*) Corolla (green), C(3)G (red), and DNA (gray). The insets show magnifications of the outlined regions displayed in the *Left*. (*E*) Immunofluorescence images showing expression of Corolla (Corolla-GFP) and C(2)M [HA-C(2)M] in midprophase I (stages 6 and 7) after depletion of Sfmbt. C(2)M colocalizes to a subset of polycomplexes during SC disassembly (stage 7) after germ line depletion of Sfmbt. Yellow arrowheads highlight the polycomplexes in stage 6 and 7 egg chambers. Corolla (Corolla-GFP; green), C(2)M [HA-C(2)M; red], and DNA (gray). Images shown in *E* are the same as those shown in *SI Appendix*, Fig. S5*A*. nanos-Gal4 was used to drive germ line–specific expression of shRNAs. For control RNAi, mCherry RNAi was used. Corolla corresponds to an endogenously expressed GFP-tagged transgene; endogenous C(3)G was detected with an antibody and C(2)M with an HA antibody. Stg, stage. (Scale bar for all images: 3 μm.)

dramatically during oogenesis, forming an extensive three-dimensional network of Corolla-positive filaments within the nucleus of stage 8/9 oocytes (Fig. 1*B*) (Movie S2), whereas almost no filaments could be detected in the control oocytes (Movie S1). Supporting the hypothesis that these Corolla-positive filaments are abnormal SC structures, they also contained the SC component C(3)G (Fig. 1*D* and *SI Appendix*, Fig. S2*A*), a subset incorporated the SC component C(2)M (Fig. 1*E* and *SI Appendix*, Fig. S5*A*; see quantification in *SI Appendix*, Fig. S5 *B* and *C*), and depletion of c(3)G impaired filament formation after depletion of Sfmbt (no polycomplex formation [0%] after coexpression of c(3)G RNAi and Sfmbt RNAi-1, using the nanos-Gal4 driver and the Corolla-GFP reporter for filaments visualization; $n = 24$ egg chambers [stage 5], and $n = 47$ [stages 6 to 8]). The Corolla-positive filaments will therefore be referred to as polycomplexes from here onward.

Careful analysis of polycomplex formation after depletion of Sfmbt showed that during early diplotene (stages 5 to 7), many polycomplexes were in close association with the oocyte DNA (Fig. 1*B*). This occurred not only within centromeric regions of the oocyte but also along the chromosome arms (Movie S3). Altogether, our results fully confirm that Sfmbt is required to avoid the formation of polycomplexes during diplotene.

The Polycomplexes Formed after Depletion of Sfmbt Have a Well-Defined Periodic Structure and Are Extremely Dynamic. Polycomplexes correspond to abnormal SC structures with a well-defined periodic organization. In *C. elegans*, these complexes are highly dynamic, and their assembly is promoted by weak hydrophobic interactions (45). In *Drosophila*, mutants for E3 ubiquitin-protein ligase *seven in absentia (sina)* show polycomplex formation during SC assembly (pachytene) (44). In order to investigate if the polycomplexes formed after depletion of Sfmbt are similarly periodic and dynamic, we performed superresolution microscopy and live-cell imaging analysis of these structures. We observed that these diplotene polycomplexes had a well-defined periodic crystal-like structure, with repetitive 140-nm intervals between Corolla layers (Fig. 2*A*). We also observed that these crystal-like structures were remarkably dynamic, with apparent filament fusions and formation of circular structures, and that they were frequently associated with the meiotic chromatin (Fig. 2*B*) (Movies S4 and S5). Please note

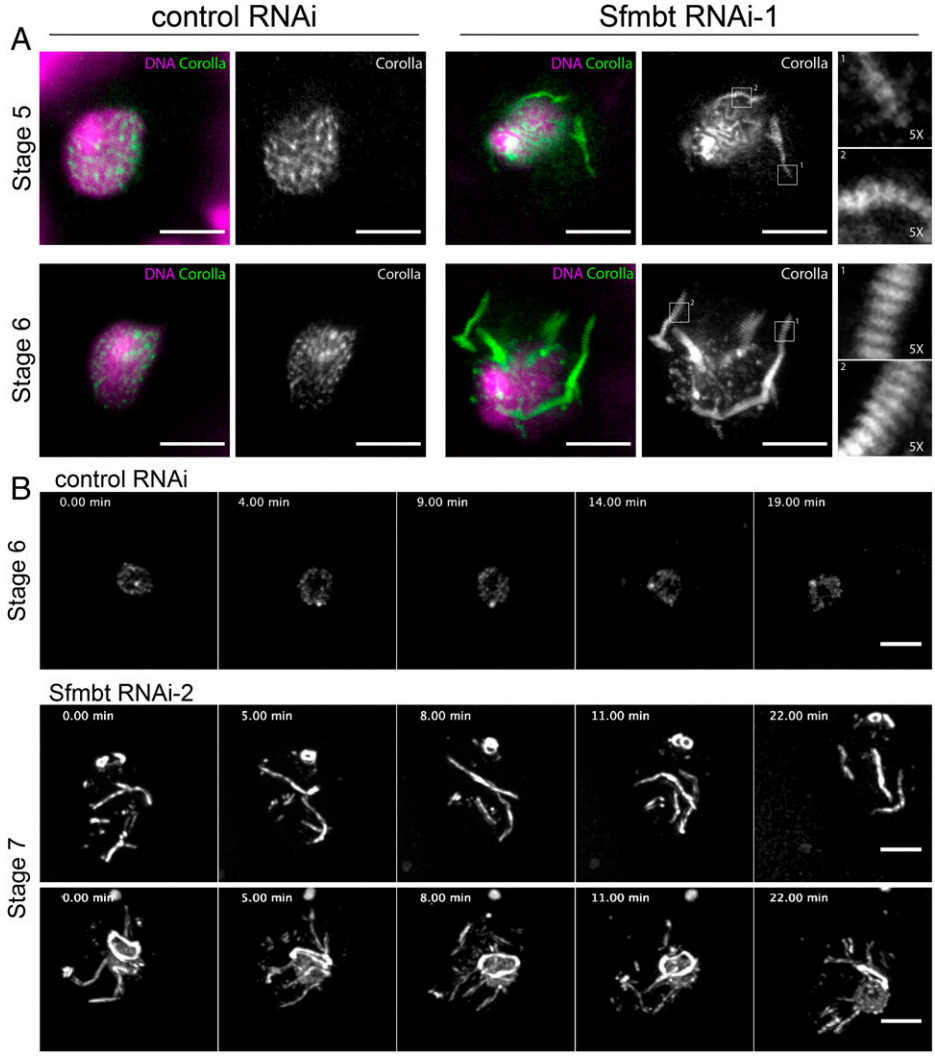

Fig. 2. The polycomplexes formed after depletion of Sfmbt have a well-defined periodic structure and are extremely dynamic. (*A*) CH-STED superresolution images of the polycomplexes formed during midoogenesis (stages 5 and 6) after depletion of Sfmbt. Polycomplexes show a highly repetitive stacked organization of SC components, with repetitive 140-nm intervals between Corolla layers. DNA (purple) and Corolla (green). The *Insets* show magnifications of the outlined regions displayed in the *Left*. (*B*) Time-lapse images of a midoogenesis oocyte nucleus containing an endogenously expressed GFP-tagged Corolla transgene. Images were taken every 1 min to evaluate polycomplex dynamics (see Movies S4 and S5). nanos-Gal4 was used to drive germ line–specific expression of shRNAs. For control RNAi, mCherry RNAi was used. (Scale bar for all images: 3 μm.)

that for stage 7 control oocytes, Corolla-GFP signal was typically insufficient for live-cell imaging due to increased disassembly of the SC. Our results suggest that, albeit formed at different stages of *Drosophila* oogenesis, the polycomplexes formed in *sina* mutants or after depletion of Sfmbt share a common periodic structure. Furthermore, they also suggest that similar to *C. elegans*, these polycomplexes are remarkably dynamic.

Sfmbt Localizes to the Supporting Nurse Cell's Chromatin and Is Efficiently Depleted by RNAi. To better understand Sfmbt expression during *Drosophila* oogenesis and the efficiency of its depletion by RNAi, we engineered a CRISPR-based knock-in of a C-terminal GFP tag within *Sfmbt* endogenous locus (*SI Appendix, Material and Methods* provides additional information). Homozygous *Sfmbt*-GFP flies were viable and fertile, without any obvious phenotypes. Since *Sfmbt* is an essential gene (36), this demonstrated that the function of this protein is not significantly affected by the fusion of a C-terminal GFP tag. Analysis of Sfmbt expression showed it is ubiquitously expressed in the germ line and in the supporting somatic cells (Fig. 3*A*). In the nurse cells and supporting somatic cells, Sfmbt expression colocalized with the DNA (Fig. 3*A*, see yellow insets). This is consistent with the fact that Sfmbt is a conserved subunit of the PhoRC (36, 38). The PhoRC binds to Polycomb Response Elements (PREs) within the DNA and helps to recruit Polycomb repressive complexes (PRC1 and PRC2) for transcriptional repression of neighboring genes (36, 38, 46–49). Sfmbt had a punctuated staining within the nurse cells (Fig. 3*A*) identical to the one previously described for other Polycomb group proteins and H3K27me$_3$ (50). We failed to detect any enrichment of Sfmbt within the oocyte meiotic chromatin (Fig. 3*A*, see red inset). As expected, the Sfmbt-GFP signal became essentially undetectable within the female germ line after germ line–specific depletion of Sfmbt (Fig. 3*B*).

Sfmbt Is a Transcriptional Repressor of SC Genes. Since Sfmbt is a conserved subunit of the PhoRC and its expression colocalized to the nurse cell's DNA (Fig. 3*A*), we reasoned that the SC disassembly defects observed after Sfmbt depletion were due to defects in nurse cell gene expression. To test this hypothesis, we analyzed the impact of germ line depletion of Sfmbt in the transcriptome of young ovaries (from 2-d-old females after pupae eclosion) by RNA-seq (*SI Appendix, Material and Methods* provides additional information). These ovaries were mostly composed of mid/late prophase I egg chambers.

Germ line depletion of Sfmbt was associated with significant gene expression changes within the ovaries (*SI Appendix*, Table 1*A*). Expression misregulation was considered significant when the false discovery rate (FDR) was below 0.05 [$-\log_2(\text{FDR}) \geq 4.3$]. For genes with FDR < 0.05 and $\log_2$(fold change [FC]) > 1, there were 595 and 459 genes whose expression was up-regulated and down-regulated, respectively, after depletion of Sfmbt. For genes with FDR < 0.05 and $\log_2(\text{FC}) > 2$, there were 349 and 90 genes whose expression was up-regulated and down-regulated, respectively, after depletion of Sfmbt. The fact that the number of strongly up-regulated genes was bigger than the number of strongly down-regulated genes is consistent with the fact that Sfmbt is a canonical repressor of transcription.

Expression of several components of the SC was significantly up-regulated after germ line depletion of Sfmbt (Sfmbt RNAi-1) (Fig. 4*A*, see genes in red) (*SI Appendix*, Fig. S4*A* and Table 1 *A* and *C*). Supporting the hypothesis that Sfmbt RNAi polycomplex phenotype is not related to *sina* defects, expression of this E3 ubiquitin ligase was not affected by Sfmbt depletion (Fig. 4*A*, see gene in green). Consistent with our previous Sfmbt-GFP results, where the germ line expression of Sfmbt was significantly reduced after depletion of Sfmbt (Fig. 3*B*), expression of *Sfmbt* messenger RNA (mRNA) was also significantly reduced after Sfmbt RNAi (Fig. 4*A*, see gene in blue).

The RNA-seq results were further confirmed by RT-ddPCR for absolute quantification of transcript levels. Our RT-ddPCR analysis confirmed that several SC genes were significantly up-regulated after Sfmbt RNAi (Fig. 4*B*), with *ord*, *c(3)G*,

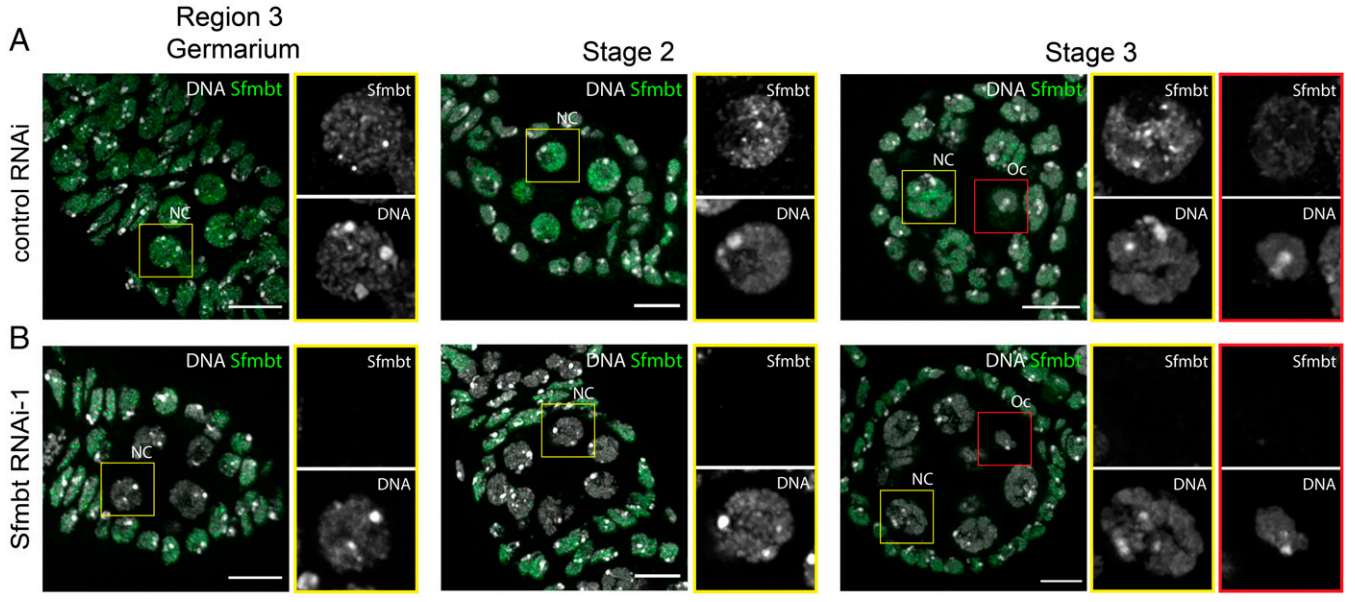

Fig. 3. Sfmbt localizes to the supporting nurse cell's chromatin, and it is efficiently depleted by RNAi. Immunofluorescence images of Sfmbt expression (Sfmbt-GFP) in early oogenesis for both control RNAi and Sfmbt RNAi. (*A*) In control RNAi, Sfmbt has a distinctive punctuated staining in the nurse cell's chromatin during early oogenesis. Sfmbt is detectable in the oocyte nucleus, but it is not enriched in oocyte chromatin. (*B*) There is no detectable expression of Sfmbt in either the nurse cells or the oocyte nucleus after Sfmbt RNAi. DNA (white) and Sfmbt (green). The insets show magnifications of the outlined regions shown in the *Left*. Nurse cells (yellow outlined region), oocyte (red outlined region). All results use the germ line–specific nanos-Gal4 driver for expression of shRNAs. For control RNAi, mCherry RNAi was used. *Sfmbt*-GFP was endogenously tagged by CRISPR. NC, nurse cell; Oc, oocyte. (Scale bar for all images: 10 μm.)

corona, and *corolla* up-regulated 104.08-fold (±15.81), 5.46-fold (±0.66), 10.45-fold (±3.13), and 2.70-fold (±0.28), respectively. Expression of SC gene *c(2)M* was not significantly up-regulated after Sfmbt RNAi [1.08-fold (±0.02)]. We also confirmed the efficient depletion of *Sfmbt* [0.22-fold (±0.06)]. The functional relevance of SC gene overexpression was further supported by the fact that C(3)G protein levels were similarly strongly up-regulated after Sfmbt RNAi (*SI Appendix*, Fig. S4*D*).

Since the female germ line epigenome is highly dynamic during prophase I (35, 50) and SC genes are transiently transcribed during early prophase I (7), we reasoned that Sfmbt likely has an important role in the epigenetic regulation of prophase I genes, including the transcriptional repression of SC genes during mid/late prophase I.

Sfmbt Is Necessary during Mid/Late Prophase I for Avoidance of Polycomplex Formation. Germ line transcription of SC genes mostly occurs during the cystoblast mitotic divisions and early prophase I (8-/16-cell cysts) (7, 19), just before the full assembly of the SC at pachytene. We reasoned that Sfmbt is a transcriptional repressor of SC genes during mid/late prophase I and their unrestrained expression after Sfmbt depletion is associated with polycomplex formation after the onset of SC disassembly (diplotene). Yet, since the nanos-Gal4 driver is capable of inducing a strong expression of UAS-containing transgenes already within the germ line stem cells and the dividing cystoblasts (42), we decided to use the matTub-Gal4 driver for germ line depletion of Sfmbt to confirm our hypothesis.

The matTub-Gal4 induces germ line expression of UAS-containing transgenes only after region 3 of the germarium (pachytene), mostly bypassing the premeiotic mitotic divisions and early prophase I (51). To avoid other confounding factors, we performed this experiment in the absence of the Corolla-GFP reporter. We observed that similar to the nanos-Gal4 (*SI Appendix*, Fig. S2*A*, see yellow arrowheads), depletion of Sfmbt using the matTub-Gal4 was similarly associated with polycomplex formation during SC disassembly (*SI Appendix*, Fig. S3*A*, see yellow arrowheads; see quantification in *SI Appendix*, Fig. S3*B*). This supports the hypothesis that Sfmbt-dependent repression of SC expression is mostly necessary during mid/late prophase I for avoidance of polycomplex formation.

Sfmbt and Distinct Polycomb Subunits Repress SC Gene Transcription. We reasoned that Sfmbt regulates the expression of SC genes and other prophase I genes through PhoRC and its recruitment of the repressive complex PRC2 for transcriptional repression of target genes. Since *E(z)* encodes the catalytic component of PRC2 (52), we tested if the ovarian transcriptome was similarly affected by depletion of Sfmbt or E(z). Consistently, we observed a significant identity overlap of misexpressed genes after germ line depletion of Sfmbt or E(z) (*SI Appendix*, Fig. S4*C*; $P < 10^{-16}$ and $P = 4.5 \times 10^{-13}$ for identity of up-regulated and down-regulated genes, respectively). This overlap included the SC gene *ord* that was similarly up-regulated after Sfmbt RNAi or E(z) RNAi (Fig. 4*F* and *SI Appendix*, Fig. S4*B* and Table 1*B*).

Germ line depletion of Pho, the interacting subunit of Sfmbt within the PhoRC, was also associated with a significant expression up-regulation of SC genes *ord*, *c(3)G*, and *corolla* (Fig. 4*F* and *SI Appendix*, Fig. S4*B*), whereas depletion of Sex comb on midleg (Scm), a protein that links PhoRC and other Polycomb complexes, was similarly associated with an up-regulation of *ord* expression. Interestingly, and further confirming the role of these Polycomb subunits in the regulation of SC gene expression, germ-line depletion of Pho and Scm was similarly associated with polycomplex formation during SC disassembly (Fig. 1*A*; see quantification in Fig. 1*C*). Although these polycomplexes were significantly smaller than the ones observed after *Sfmbt* RNAi (Fig. 1*A*), they were nevertheless also detected without the Corolla-GFP reporter (*SI Appendix*, Fig. S2*B*).

However, not all prophase I genes or even SC genes were similarly affected by depletion of Sfmbt or other subunits of the Polycomb group complex (Fig. 4*F* and *SI Appendix*, Fig. S4 *B* and *C*). For example, whereas *ord* was significantly up-regulated by the depletion of distinct Polycomb subunits, *c(3)G* and *corolla* were only significantly up-regulated after depletion of Sfmbt or Pho (Fig. 4*F*).

Expression of the SC Gene Corona Is Directly Regulated by Sfmbt. PhoRC and Polycomb group proteins bind an overlapping set of ∼400 genes highly enriched for transcription factors (53). Sfmbt RNAi could indirectly regulate SC genes by repressing a transcription factor that activates SC genes. Alternatively, Sfbmt could associate with SC genes to directly repress their expression. To discriminate between these possibilities, we used chromatin immunoprecipitation sequencing (ChIP-seq) to measure the association of Sfmbt and its binding partner Pho throughout the genome. We used an antibody recognizing Pho in wild-type flies or an antibody recognizing GFP in GFP-Sfmbt flies (*SI Appendix*, Table 1*F*). As a negative control, we performed GFP ChIP on wild-type (Oregon-R) flies lacking GFP. GFP-Sfmbt and Pho associated with hundreds of shared binding sites. Despite differences in ChIP efficiency, the relative signal of Pho and GFP-Sfmbt at each site was highly correlated, suggesting that Pho and Sfmbt bind the same sites on DNA as a complex (Fig. 4*E*). Pho and Sfmbt associated with 289 different genes, including known sites in the two major Hox clusters, *Bx-c* and *Ant-c* (Fig. 4*E*) (*SI Appendix*, Table 1*G*). Pho and Sfmbt were also enriched near the *corona* promoter but not near other SC genes (Fig. 4*C* and *SI Appendix*, Fig. S6*B*). H3K27me$_3$ deposited by PRC2 was enriched on *corona* (Fig. 4*C*) and other target genes with high Sfmbt/Pho enrichment (Fig. 4*D*). Sites with lower Sfmbt/Pho enrichment lacked significant H3K27me$_3$ signal (Fig. 4*D*). Although Sfmbt/Pho bound to 289 different genes in ovaries, only six of these genes, including *corona*, were significantly up-regulated and expressed in Sfmbt RNAi (log2 FC > 3, TPM > 3) (*SI Appendix*, Fig. S6*A*). Three of the other five genes, *goosecoid, chinmo*, and *CG9650,* encode transcription factors that may indirectly contribute to gene misregulation in Sfmbt RNAi. We concluded that Sfmbt directly represses a small number of genes, including the SC component *corona*, to prevent polycomplex formation.

Up-regulation of Corona Expression Is Sufficient to Induce the Formation of Polycomplexes during SC Disassembly. If up-regulation of SC gene expression after depletion of Sfmbt is the reason why polycomplexes are formed during SC disassembly, then ectopic expression of these genes using the UAS/Gal4 system should phenocopy Sfmbt RNAi. We focused our initial analysis on the SC gene *corona*, as its expression is directly regulated by Sfmbt (Fig. 4 *A* and *C*). Consistently, overexpression of *corona* (Fig. 5*D*) [UAS-*corona* (24)], using the nanos-Gal4 germ line driver and in the absence of the Corolla-GFP reporter, was sufficient to induce the formation of polycomplexes during SC disassembly (Fig. 5*A*; see quantification in Fig. 5*B*).

Further supporting the hypothesis that polycomplex formation after depletion of Sfmbt is due to increased levels of SC gene expression, an increase in corolla gene copy number (three copies

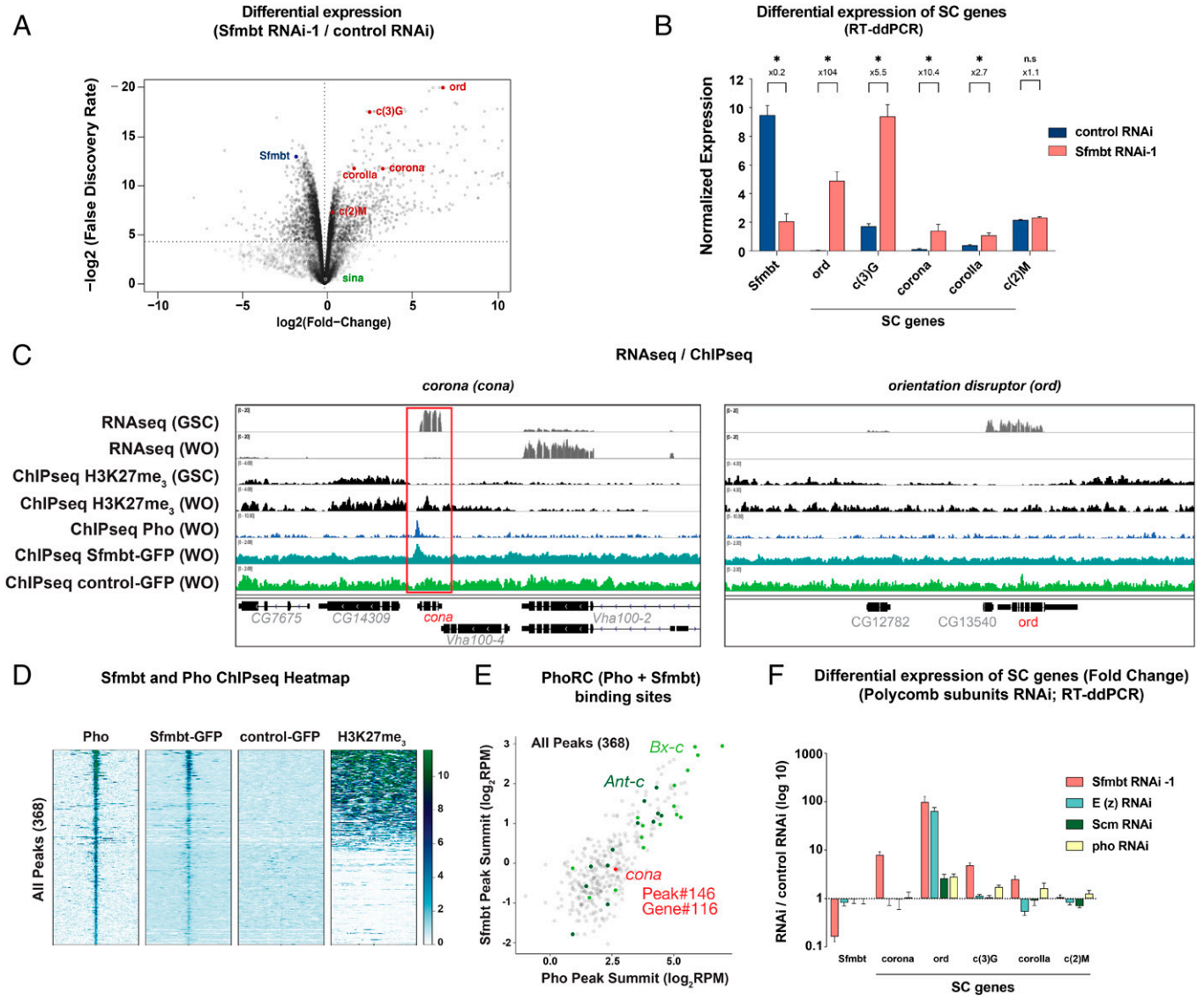

Fig. 4. Sfmbt is a general repressor of SC gene expression during prophase I and directly regulates transcription of *corona* (cona). Germ line–specific depletion of Sfmbt leads to significant up-regulation of SC gene expression during prophase I. PhoRC, whose subunits include Sfmbt and Pho, shows significant binding enrichment to the corona promoter. (*A*) RNA-seq analysis of polyA-enriched RNA from 2-d-old female ovaries (after pupae eclosion). Volcano plot depicting the log2 FC of gene expression (Sfmbt RNAi compared to control RNAi) against the −log2 of the FDR in a differential expression analysis. The dashed horizontal line represents FDR = 0.05. SC genes [*ord*, *c(3)g*, *corolla*, *corona*, and *c(2)M*] are shown in red, *sina* in green, and *Sfmbt* in blue. Detailed information is provided in *SI Appendix*, Table 1*A*. (*B*) RT-ddPCR analysis of *Sfmbt* and SC genes' transcript levels from 2-d-old female ovaries. Expression fold exchange of each gene is displayed on the top of each bar (Sfmbt RNAi compared to control RNAi). Average ± SD of five biological replicas for *ord*, *c(3)g*, *corolla*, and *corona* analysis and two biological replicas for *c(2)M* analysis. Statistically significant differences are marked with * ($P = 0.0079$, multiple Mann-Whitney test). (*C*) Genome Browser tracks from RNA-seq (top two tracks) and ChIP-seq (bottom five tracks) experiments showing 25 kb from the *corona* and *ord* loci. Scale in reads per million is indicated. WO (whole ovary material), including nurse cells and oocytes. GSC (germ cell progenitor material) purified from bam mutant ovary. Both *corona* (*cona*) and *ord* show a repression of gene expression in WO compared to GSC. However, *cona* is the only SC gene with a significant enrichment of $H3K27me_3$, as well as binding of PhoRC subunits Pho and Sfmbt (highlighted in red box). Pho and Sfmbt-GFP ChIP-seq for *corona* (*cona*) and *ord* are the same as shown in *SI Appendix*, Fig. S6*B*. RNA-seq for GSC and $H3K27me_3$ ChIP-seq datasets were originally published in DeLuca et al. (50). (*D*) Heatmap of indicated ChIP signal from whole ovaries showing 6 kb encompassing all Pho and Sfmbt peaks called by MACS2. GFP-control corresponds to anti-GFP ChIP performed on untagged strain. (*E*) Reads per million (RPM) signal at the summit of each MACS2-called peak for Pho and Sfmbt ChIP. Note the strong correlation between peak heights in GFP and Pho ChIP despite the significantly higher background in the GFP ChIP. Peaks residing in the Antennapedia (Ant-c) and Bithorax (Bx-c) gene complexes are indicated (in dark and light green, respectively). A peak in *corona* (*cona*) (red) places it in the top 1% of *Drosophila* genes bound by *PhoRC*. (*F*) Differential expression of SC genes (FC) after germ line–specific depletion of Sfmbt and other Polycomb proteins. Average ± SD of two biological replicas.

of corolla: two endogenous and one corresponding to a genomic BAC transgene) was sufficient to enhance the polycomplexes' phenotype observed after Sfmbt RNAi, with a significant increase in the size of formed polycomplexes (Fig. 5*C*). An increase in corolla copy number (three copies of corolla) was, per se, not sufficient to induce significant formation of polycomplexes (compare control RNAi results in Fig. 1*C*, with three copies of corolla, and *SI Appendix*, Fig. S2*B*, without an extra copy of corolla).

Sfmbt Is Required for Normal Meiosis and Female Fertility. Sfmbt is essential for the correct expression of distinct prophase I genes, including the transcriptional repression of SC genes during mid/late prophase I and avoidance of polycomplex formation during SC disassembly. While E(z) and Su(z)12, two key subunits of PRC2, are essential for maintaining oocyte fate and female fertility (50, 54, 55), the requirement of other Polycomb group subunits within the female germ line is less clear.

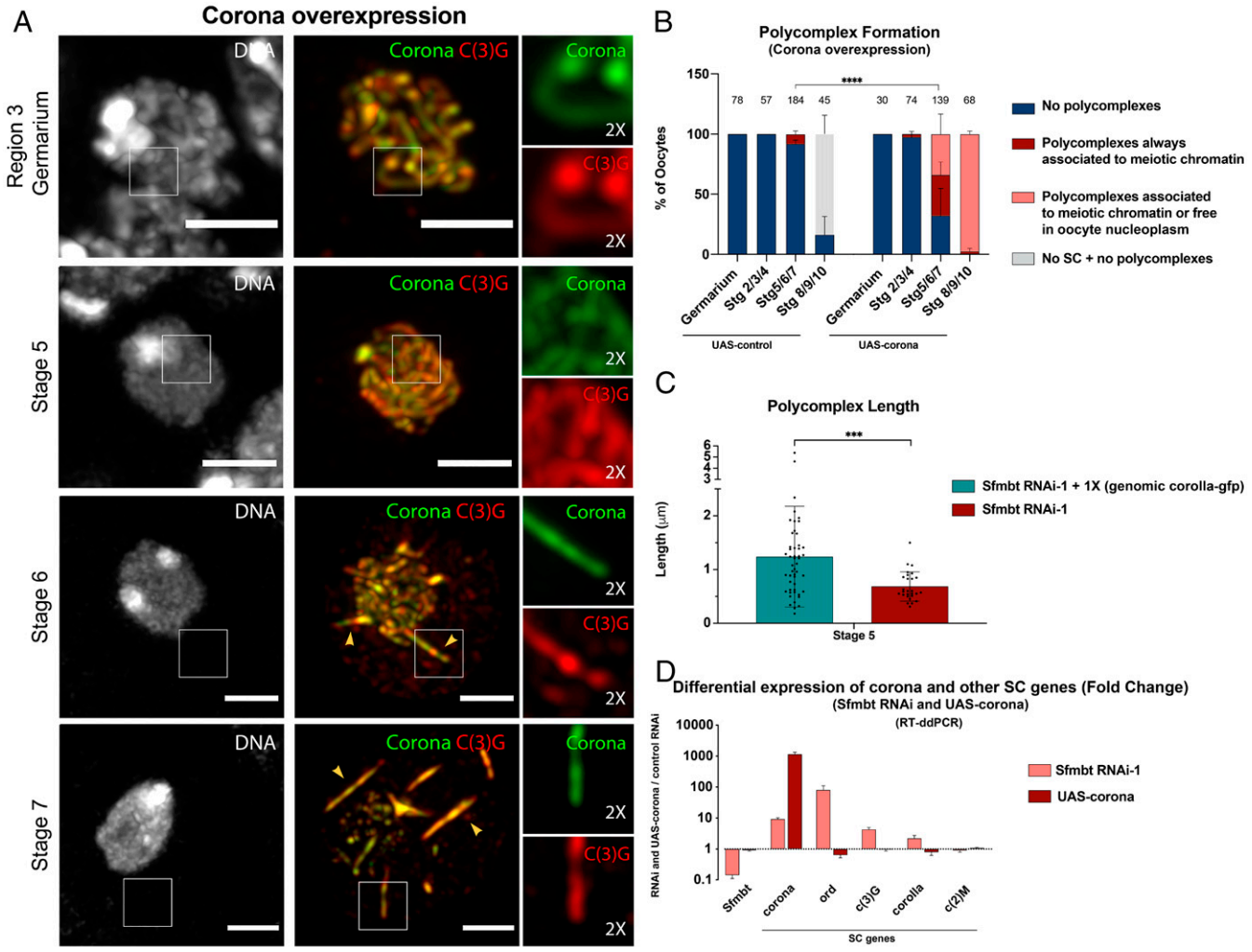

Fig. 5. Up-regulation of *corona* (cona) expression is sufficient to induce polycomplex formation during SC disassembly. (*A*) Immunofluorescence images showing the formation of abnormal SC structures (polycomplexes) after up-regulation of SC component Corona expression. Similar to Sfmbt RNAi (see Fig. 1), polycomplex formation only occurs during mid/late prophase I (SC disassembly) (stages 6 and 7) but not during early prophase I (pachytene; SC assembly) (region 3 of the germarium). Yellow arrowheads highlight the polycomplexes in stage 6 and 7 egg chambers. Corona (green), C(3)G (red), and DNA (gray). The insets show magnifications of the outlined regions shown in the left panels. (*B*) Quantification of polycomplex formation after Corona overexpression was done using staining for endogenous C(3)G. Number of scored oocytes is displayed on the top of each bar. Statistically significant differences are marked with **** ($P < 0.0001$, Fisher's exact test). Average ± SD of three biological replicas. Control datasets are the same as the ones shown in *SI Appendix*, Fig. S2*B*. (*C*) Quantification of polycomplex length after Sfmbt depletion with or without an additional genomic copy of Corolla (genomic BAC transgene; *corolla*-GFP) was done using staining for endogenous C(3)G. The length of polycomplexes increased with the presence of an additional genomic copy of Corolla. Statistically significant differences are marked with *** ($P = 0.0003$, Mann-Whitney test). Average ± SD of two biological replicas. (*D*) Differential expression of *corona* and other SC genes (FC) after germ line–specific depletion of Sfmbt and UAS-*corona*-Venus overexpression. Average ± SD of two biological replicas. nanos-Gal4 was used to drive germ line–specific expression of Corona (UAS-*corona*-Venus). Stg, stage. (Scale bar for all images: 3 μm.)

Adult females whose germ line was depleted for Sfmbt were sterile, with significant metaphase I defects (Fig. 6 *A* and *B*), reduced egg laying (Fig. 6*C*), eggshell length defects (short eggs) (Fig. 6*D*), and reduced egg hatching (Fig. 6*E*). Contrary to depletion of Salsa RNA helicase (56) and mutants for meiotic DNA repair (57, 58), depletion of Sfmbt was not associated with significant dorsal-ventral patterning defects of the eggshell (fused dorsal appendages; Fig. 6*D*; class 2 and 3) or abnormal morphology of the oocyte karyosome (Fig. 1 *A* and *B*), which suggests that Sfmbt is not critical for the correct repair of meiotic DSBs. We reasoned that Sfmbt regulates the expression of distinct female germ line genes, some negatively and others positively, and that the phenotypes observed after depletion of Sfmbt are a consequence of transcriptional misregulation of multiple genes, including the abnormal up-regulation of SC genes during mid/late prophase I. Our results therefore support the pivotal role of Sfmbt in the regulation of gene expression during female gametogenesis.

Discussion

Sfmbt Prevents the Formation of Polycomplexes during Diplotene by Avoiding the Unrestrained Expression of SC Genes. We showed that the Polycomb group protein Sfmbt, the *Drosophila* ortholog of human MBTD1 and L3MBTL2, is crucial to prevent excessive expression of SC genes and polycomplex formation during diplotene. Analysis of these polycomplexes showed that they contain distinct SC components, are extremely dynamic, and have a well-defined periodic crystal-like structure, with repetitive 140-nm intervals between Corolla layers. Since the *Drosophila* SC has ∼120- to 130-nm width (25), our results are consistent with the model showing that the diplotene polycomplexes, like the ones previously described during pachytene (44), correspond to stacked layers of SC complexes.

Formation of polycomplexes after germ line depletion of Sfmbt occurred during diplotene, whereas SC assembly during

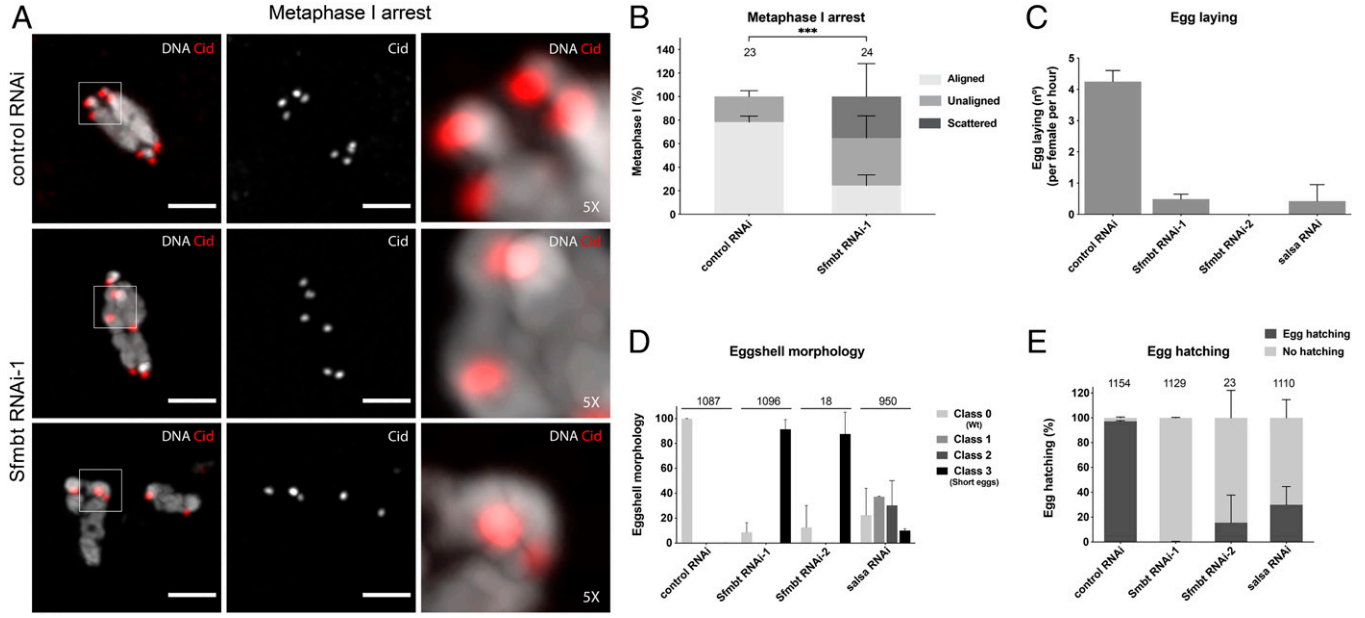

Fig. 6. Sfmbt is required for normal meiosis and female fertility. (*A*) Immunofluorescence images showing abnormal metaphase I arrest after germ line depletion of Sfmbt. DNA (white) and Cid (red). The *Insets* show magnifications of the outlined regions displayed in the *Left*. (*B*) For scoring of metaphase I defects in stage 13 and 14 oocytes, three different phenotypic classes were established (aligned, depicted in control image; unaligned, depicted in the upper Sfmbt RNAi image; and scattered, depicted in the bottom Sfmbt RNAi image) using DNA staining and the centromeric protein Cid. Number of scored oocytes is displayed on the top of each bar. Statistically significant differences are marked with *** ($P < 0.0001$, Fisher's exact test). Average ± SD of two biological replicas. (*C*) Egg laying was significantly reduced after germ line depletion of Sfmbt. Depletion of Salsa (salsa RNAi) was used as a positive control for reduced egg laying (56). Average ± SD of two biological replicas. (*D*) Quantification of eggshell dorsal appendage defects. Eggs laid by females whose germ line was depleted for Sfmbt were typically short (class 3: short eggs). Depletion of Salsa was used as a positive control for eggshell dorsal-ventral patterning defects (56). Phenotypic classes are identical to the ones reported in Rathore et al. (56). Number of scored eggs is shown on the top of each bar. Average ± SD of two biological replicas. (*E*) Female fertility (egg hatching) was significantly reduced after depletion of Sfmbt. Female fertility was calculated by the frequency of egg hatching 48 h after oviposition. *n* represents the total number of eggs counted in both biological replicas. Average ± SD of two biological replicas. Number of scored eggs is shown on the top of each bar. nanos-Gal4 was used to drive germ line–specific expression of shRNAs. For control RNAi, mCherry RNAi was used. (Scale bar for all images: 3 μm.)

pachytene was normal without polycomplex formation. Likewise, overexpression of the SC component Corona, using the Gal4/UAS system and the germ line–specific nanos-Gal4 driver, was only sufficient to induce polycomplex formation during diplotene. Since the nanos-Gal4 driver already induces a strong expression of UAS-containing transgenes within germ line stem cells and the differentiating cystoblasts (42), we reasoned that an unknown mechanism capable of avoiding polycomplex formation during pachytene likely exists. An obvious candidate is E3 ubiquitin-protein ligase Sina, whose function was recently reported to be important to avoid polycomplex formation during SC assembly (pachytene) (44). Polycomplexes may form at diplotene when nucleoplasmic Corona produced after Sfmbt RNAi or by UAS-corona interacts with SC components, leaving meiotic chromatin. The ability of Corona to "seed" polycomplexes could be related to its normal function in promoting the assembly of C(3)G transverse filaments during pachytene (24).

SC Gene Transcription Is Regulated by Distinct Polycomb Subunits. The precise mechanism by which the Polycomb group proteins regulate gene expression during female gametogenesis is still remarkably poorly understood, as the requirements of the different subunits can vary dramatically. Whereas E(z) and Su(z)12, two key subunits of PRC2, are essential to maintain oocyte fate and repress hundreds of genes in nurse cells (50, 54, 55), other Polycomb group proteins appear to regulate far fewer genes and have more subtle developmental phenotypes. For example, RNAi depletion or a null mutant allele for *Polycomb* (*Pc*), a conserved subunit of PRC1, up-regulates a small number of Polycomb target genes, such as *chinmo*, but does not show obvious oocyte or fertility defects (50, 55).

A second class of genes including Scm, Sfmbt, and Pho represses more Polycomb targets than Pc and prevents polycomplex formation during diplotene. Sfmbt and Pho form PhoRC (36, 38), which binds regulatory DNA around Polycomb target genes (36, 38, 46–49). We did not find sites highly enriched for Sfmbt but without Pho or highly enriched for Pho but without Sfmbt, suggesting that both proteins bind chromatin as a single complex. Therefore, why is the polycomplex phenotype after Sfmbt RNAi stronger than Pho RNAi? Pho function in PhoRC might be partially complemented by Pho-like, a Pho paralog highly expressed in nurse cells. Additionally, Sfmbt may bring PhoRC to target genes through direct interaction with chromatin or through interactions with other transcription factors besides Pho (59, 60).

Scm links PhoRC to PRC1 and PRC2 (46, 47) and enriches PRC1 and PRC2 on target genes in nurse cells (50). If Scm recruits PRC2 to Sfmbt-bound sites, why would PRC2 depletion [e.g., E(z) RNAi] have a stronger and qualitatively different phenotype (55) than depletion of Sfmbt? A simple explanation is that PRC2 represses both PhoRC-bound genes and other genes not bound by PhoRC. In nurse cells, most PRC2-repressed genes are not highly enriched in $H3K27me_3$ or PhoRC (50). Many of these genes are expressed in nurse cell progenitors, suggesting that PRC2 is generally important for repressing previously active genes. While some progenitor-specific genes may be turned off by PhoRC, others may be deactivated through other repressors and/or the loss of activators.

To consolidate our results with previous findings, we propose the following working model for Polycomb-dependent gene silencing in *Drosophila* germ line development. As mitotic progenitors differentiate into oocytes and nurse cells, many

progenitor-expressed genes, including some SC components, must be deactivated. Some progenitor-expressed genes are repressed by PhoRC, while others are repressed by other transcription factors. Some may be repressed by both. However, both types of repressors can be enhanced by PRC2 activity. At PhoRC-bound genes, Scm concentrates additional PRC2 (and PRC1) to further enhance repression. We propose that this multilayered regulatory mechanism most likely evolved to achieve quantitatively different amounts of repression of different target genes during female gametogenesis.

Prophase I Expression of SC Gene corona Is Directly Regulated by PhoRC. *corona* was the only SC gene with a robust enrichment of Sfmbt and Pho binding on its promoter. However, other SC genes, notably *ord* and *c(3)G*, did not show Sfmbt or Pho enrichment but were significantly up-regulated after Sfmbt RNAi. We identified three genes, *chinmo*, *CG9650*, and *Goosecoid*, that were bound by Sfmbt, whose expression was up-regulated after Sfmbt RNAi, and that encode transcription factors. These transcription factors may potentially regulate *ord*, *c(3)G*, and many other up- and down-regulated genes in Sfmbt RNAi. Thus, in addition to its important function in preventing polycomplex formation during diplotene, Sfmbt may also regulate other important germ line processes. Finally, we propose that some germ line genes may be similarly regulated by Polycomb proteins in *Drosophila* and mammals. Analysis of a publicly available gene expression dataset from mouse oocytes mutant for PRC1 (61) detected a significant up-regulation of several SC gene expressions during female gametogenesis.

Materials and Methods

Additional information is provided in *SI Appendix, Material and Methods*.

***Drosophila* Husbandry and Crosses.** *Drosophila melanogaster* flies were raised at 25 °C using standard techniques. *Drosophila* husbandry, crosses, and genetics were performed at 25 °C, as previously described (35, 56, 62, 63).

***Drosophila* Stocks.** All stocks used in this work are indicated in *SI Appendix*, Table 1*D*. Germ line depletion of Sfmbt was obtained using two different nonoverlapping short hairpins: Sfmbt RNAi-1 and Sfmbt RNAi-2. Sfmbt RNAi-1 stock is available at BDSC (BL32473) (43). Sfmbt RNAi-2 stock was custom-made. A nonoverlapping short hairpin against *Sfmbt* (CG16975) was designed using an algorithm that minimizes off-target effects (64). Scm, pho, and E(z) RNAi stocks are available at BDSC. Other stocks used in this work include UAS-*corona*-Venus (24), *corolla*-GFP (39), and UAS-HA-*c(2)M* (22). A short hairpin against *mCherry* (BL35785) was used as a negative control. A short hairpin against *salsa*/CG31368 (56) was used as a positive control in some experiments. For all experiments, a minimum of two biological replicas were performed.

***Sfmbt*–enhanced GFP–CRISPR *Drosophila* Stocks.** CRISPR-mediated mutagenesis was performed by WellGenetics Inc. using the modified methods of Kondo and Ueda (65).

Egg Laying, Eggshell Phenotypes, and Egg Hatching. Eggshell phenotypes, egg hatching, and egg laying experiments were performed as previously described (35, 56, 62, 63). For egg laying, eggs were collected every day for 6 h, and the number of eggs was counted.

Ovary Immunostaining. Adult ovaries were processed according to standard procedures (35, 62, 63). Images were acquired using a Zeiss LSM710 Confocal microscope and the Leica laser scanning confocal microscope TCS SP8, deconvolved using Huygens Software (Scientific Volume Imaging B.V.), projected using Fiji Software, and treated with Adobe Photoshop 2017 (Adobe Microsystems). Three-dimensional projections were generated with LAXs software from immunofluorescence images acquired using the Leica laser scanning confocal microscope TCS SP8. In Coherent-hybrid STED (CH-STED) Superresolution Imaging, 90% glycerol, 0.5% *N*-propyl gallate, and 20 mM Tris·HCl (pH 8) were used as mounting medium. The superresolution CH-STED images were acquired using Abberior Instruments "Expert Line" gated-STED coupled to a Nikon Ti microscope, an oil-immersion 60× 1.4 numerical aperture Plan-Apo objective (Nikon, Lambda Series), and a pinhole size of 0.8. The coherent-hybrid mode was previously described (66) and is set by imprinting a bivortex phase map ($\rho = 0.92$) onto a spatial light modulator (Hamamatsu LSH 0801392). Used antibodies are shown in *SI Appendix*, Table 1*F*.

Signal Analysis and Quantification of Polycomplexes. For quantification of polycomplex numbers, the wide-field upright microscope AxioImager Z1 (Carl Zeiss) was used with a Plan-Apochromat 63x/1.40 Oil DIC objective. Immunofluorescence quantification of polycomplex length was performed manually using Fiji image-processing software, and z-stacks were analyzed individually from confocal microscope images.

Time-Lapse Imaging. For live-cell imaging of egg chambers, ovarioles were dissected in Schneider medium (Sigma-Aldrich) supplemented with 20% (vol/vol) fetal bovine serum (Invitrogen) and 200 mg/mL insulin (Sigma-Aldrich). To improve imaging, egg chambers were immobilized in a low-melting 0.8% agarose solution. Time-lapse imaging analysis was performed on the Leica laser scanning confocal microscope TCS SP8 (Leica Microsystems). z-Stacks were acquired at 1-μm steps every 1 min with a PL APO 63X immersion glycerol objective. Movies were processed as described in the ovary immunostaining section.

Meiotic Metaphase I Arrest Analysis. For analysis of metaphase I arrest, a protocol was used to avoid *Drosophila* egg activation (67). Images were acquired and treated as described in the ovary immunostaining section. A minimum of two independent experiments were conducted for each experimental condition. Centromere labeling was done with a rat anti-Cid antibody (Claudio E. Sunkel and Sore Steffensen, University of Porto, Portugal) (*SI Appendix*, Table 1*F*).

RNA-seq Analysis. Total RNA was extracted from 2-d-old adult female ovaries, whose female germ line was specifically depleted for Sfmbt (Sfmbt RNAi-1). An RNAi hairpin against mCherry (mCherry RNAi) was used as a negative control. Three biological replicas for each condition. Total RNA extraction was performed following standard procedures (PureLink RNA Mini Kit, Ambion). The complementary DNA (cDNA) library was made using the TruSeq Stranded mRNA sample prep kit for Illumina following the manufacturer's standard protocol. cDNA library preparation and HiSeq2500 paired-end sequencing was performed by the Genomics Unit at The Centre for Genomic Regulation (Barcelona, Spain).

ChIP-seq Analysis. ChIP was performed as previously described (50). For Sfmbt ChIPseq, it used anti-GFP antibodies on chromatin prepared from GFP-Sfmbt or untagged negative control (Oregon-R) ovaries. Two biological replicas for each condition. Used ovaries were from 2-d-old females after pupae eclosion. Antibodies used are shown in *SI Appendix*, Table 1*F*. Libraries were quantified on an Agilent TapeStation and sequenced on an Illumina NextSeq500 using 50:25 paired-end reads. Reads were aligned to *Drosophila* genome release 6 using bowtie2 (68) and were q20 filtered with Samtools (69).

Differential Gene Expression Analysis. RNA-seq reads were aligned against the *D. melanogaster* BDGP release 6 genome using the STAR aligner (70). Gene-level counts were obtained using feature counts (71). Gene counts were normalized with the TMM method (72), and differential expression analysis was performed using a quasi-likelihood F-test (73), as implemented in the edgeR R package (74). For visualization purposes, we used the normalized log2(CPM) values. Coverage plots were performed with the wiggleplotr R package using bigWig files obtained from the RNA-seq alignments transformed with the deepTools bamcoverage tool with CPM normalization (75).

RT-ddPCR. Absolute transcript levels quantification was achieved with One-Step RT-ddPCR. The Bio-Rad QX200 Droplet Digital PCR System and One-Step RT-ddPCR Advanced Kit for Probes were used according to manufacturer's instructions, and assays were optimized according to MIQE guidelines (dMIQE, 2020). *Drosophila β glucuronidase* was used as reference. Used primers, forward and reverse, and 6-FAM/ZEN/IBFQ–labeled probes (Integrated DNA Technologies) are shown in *SI Appendix*, Table 1*E*.

Sodium Dodecyl Sulfate Polyacrylamide Gel Electrophoresis (SDS-PAGE) and Western Blot. Ovaries from 2- to 4-d-old adult females from both control (mCherry RNAi) and Sfmbt RNAi were used for total protein extraction. SDS-PAGE

and Western blot were performed as previously described (35). Protein samples were run on 6% or 12% SDS-PAGE gel and transferred to Hybond-ECL nitrocellulose membrane (Amersham). Protein detection was performed using an ECL Plus solution (GE Healthcare) and an ECL Hyperfilm (Amersham). Primary and secondary antibodies are shown in *SI Appendix*, Table 1*F*.

Statistical Analysis. All statistical analyses were performed using GraphPad Prism 9.0 software. D'Agostino and Pearson normality test was applied to analyze distribution normality. A 99% CI was used for all analyses.

Data, Materials, and Software Availability. The high throughput sequencing data reported in this manuscript has been deposited in Gene Expression Omnibus database, https://www.ncbi.nlm.nih.gov/geo/ (accession no. GSE176034).

ACKNOWLEDGMENTS. We are grateful to Torcato Martins for insightful scientific discussions. We also thank Cláudia Florindo for assistance in fluorescence microscopy, Margarida Neto for maintenance of *Drosophila* stock collection and technical support, and Alexandra Tavares for technical support. We acknowledge the TRiP collection at Harvard Medical School and BDSC for providing several of the *Drosophila* stocks used in this study. We acknowledge and thank Claudio E. Sunkel for antibodies. R.G.M. is supported by Portuguese national funding through Fundação para a Ciência e a Tecnologia (FCT grant refs. PTDC/BIA-BID/28441/2017 and PTDC/BIA-BID/1606/2020). B.M. and R.D.S. are both supported by Portuguese national funding through Fundação para a Ciência e a Tecnologia, respectively, PD/BD/128342/2017 (within the scope of the ProRegeM PhD program; PD/00117/2012, CRM:0027030) and DL 57/2016/CP1361/CT0019. The Light Microscopy Unit of ABC-RI was partially supported by Portuguese national funding (FCT: PPBI-POCI-01-0145-FEDER-022122). This work was developed with the support of the research infrastructure Congento (project LISBOA-01-0145-FEDER-022170). The Transgenic RNAi Project (TRiP) collection at Harvard Medical School was supported by NIH/NIGMS R01-GM084947. The funding bodies had no role in the design of this study; collection, analysis, and interpretation of data; and manuscript writing.

Author affiliations: [a]Algarve Biomedical Center Research Institute, Universidade do Algarve, 8005-139 Faro, Portugal; [b]Instituto de Investigação e Inovação em Saúde (i3S), Universidade do Porto, Porto, 4200-135 Portugal; [c]Department of Medical Sciences and Institute for Biomedicine, Universidade de Aveiro, 3810-193 Aveiro, Portugal; [d]Faculty of Medicine and Biomedical Sciences, Universidade do Algarve, 8005-139 Faro, Portugal; [e]Instituto de Medicina Molecular João Lobo Antunes, Faculdade de Medicina, Universidade de Lisboa, 1649-028 Lisboa, Portugal; [f]Associate Laboratory i4HB - Institute for Health and Bioeconomy, School of Science and Technology, NOVA University Lisbon, 2819-516 Caparica, Portugal; [g]Applied Molecular Biosciences Unit (UCIBIO), Department of Life Sciences, School of Science and Technology, NOVA University Lisbon, Caparica, 2819-516 Portugal; and [h]Department of Biology, Brandeis University, Waltham, MA 02453

1. Y. Kassir, D. Granot, G. Simchen, IME1, a positive regulator gene of meiosis in S. cerevisiae. *Cell* **52**, 853–862 (1988).
2. R. H. Lee, S. M. Honigberg, Nutritional regulation of late meiotic events in *Saccharomyces cerevisiae* through a pathway distinct from initiation. *Mol. Cell. Biol.* **16**, 3222–3232 (1996).
3. J. Bowles *et al.*, Retinoid signaling determines germ cell fate in mice. *Science* **312**, 596–600 (2006).
4. J. Koubova *et al.*, Retinoic acid regulates sex-specific timing of meiotic initiation in mice. *Proc. Natl. Acad. Sci. U.S.A.* **103**, 2474–2479 (2006).
5. A. E. Baltus *et al.*, In germ cells of mouse embryonic ovaries, the decision to enter meiosis precedes premeiotic DNA replication. *Nat. Genet.* **38**, 1430–1434 (2006).
6. M. L. Kojima, D. G. de Rooij, D. C. Page, Amplification of a broad transcriptional program by a common factor triggers the meiotic cell cycle in mice. *eLife* **8**, e43738 (2019).
7. K. Rust *et al.*, A single-cell atlas and lineage analysis of the adult *Drosophila* ovary. *Nat. Commun.* **11**, 5628 (2020).
8. P. Goldstein, Multiple synaptonemal complexes (polycomplexes): Origin, structure and function. *Cell Biol. Int. Rep.* **11**, 759–796 (1987).
9. S. E. Hughes, R. S. Hawley, Alternative synaptonemal complex structures: Too much of a good thing? *Trends Genet.* **36**, 833–844 (2020).
10. M. Sym, G. S. Roeder, Zip1-induced changes in synaptonemal complex structure and polycomplex assembly. *J. Cell Biol.* **128**, 455–466 (1995).
11. C. Merritt, G. Seydoux, The Puf RNA-binding proteins FBF-1 and FBF-2 inhibit the expression of synaptonemal complex proteins in germline stem cells. *Development* **137**, 1787–1798 (2010).
12. D. Zickler, N. Kleckner, Recombination, pairing, and synapsis of homologs during meiosis. *Cold Spring Harb. Perspect. Biol.* **7**, a016626 (2015).
13. S. E. Hughes, D. E. Miller, A. L. Miller, R. S. Hawley, Female meiosis: Synapsis, recombination, and segregation in *Drosophila melanogaster*. *Genetics* **208**, 875–908 (2018).
14. K. S. McKim *et al.*, Meiotic synapsis in the absence of recombination. *Science* **279**, 876–878 (1998).
15. A. F. Dernburg *et al.*, Meiotic recombination in *C. elegans* initiates by a conserved mechanism and is dispensable for homologous chromosome synapsis. *Cell* **94**, 387–398 (1998).
16. P. J. Romanienko, R. D. Camerini-Otero, The mouse *Spo11* gene is required for meiotic chromosome synapsis. *Mol. Cell* **6**, 975–987 (2000).
17. W. K. Leung *et al.*, The synaptonemal complex is assembled by a polySUMOylation-driven feedback mechanism in yeast. *J. Cell Biol.* **211**, 785–793 (2015).
18. S. I. Nagaoka, T. J. Hassold, P. A. Hunt, Human aneuploidy: Mechanisms and new insights into an age-old problem. *Nat. Rev. Genet.* **13**, 493–504 (2012).
19. N. Christophorou, T. Rubin, J. R. Huynh, Synaptonemal complex components promote centromere pairing in pre-meiotic germ cells. *PLoS Genet.* **9**, e1004012 (2013).
20. S. Takeo, C. M. Lake, E. Morais-de-Sá, C. E. Sunkel, R. S. Hawley, Synaptonemal complex-dependent centromeric clustering and the initiation of synapsis in *Drosophila* oocytes. *Curr. Biol.* **21**, 1845–1851 (2011).
21. S. L. Page, R. S. Hawley, c(3)G encodes a *Drosophila* synaptonemal complex protein. *Genes Dev.* **15**, 3130–3143 (2001).
22. E. A. Manheim, K. S. McKim, The synaptonemal complex component C(2)M regulates meiotic crossing over in *Drosophila*. *Curr. Biol.* **13**, 276–285 (2003).
23. L. K. Anderson *et al.*, Juxtaposition of C(2)M and the transverse filament protein C(3)G within the central region of *Drosophila* synaptonemal complex. *Proc. Natl. Acad. Sci. U.S.A.* **102**, 4482–4487 (2005).
24. S. L. Page *et al.*, Corona is required for higher-order assembly of transverse filaments into full-length synaptonemal complex in *Drosophila* oocytes. *PLoS Genet.* **4**, e1000194 (2008).
25. K. A. Collins *et al.*, Corolla is a novel protein that contributes to the architecture of the synaptonemal complex of *Drosophila*. *Genetics* **198**, 219–228 (2014).
26. M. R. Gyuricza *et al.*, Dynamic and stable cohesins regulate synaptonemal complex assembly and chromosome segregation. *Curr. Biol.* **26**, 1688–1698 (2016).
27. C. K. Cahoon *et al.*, Superresolution expansion microscopy reveals the three-dimensional organization of the *Drosophila* synaptonemal complex. *Proc. Natl. Acad. Sci. U.S.A.* **114**, E6857–E6866 (2017).
28. A. Sourirajan, M. Lichten, Polo-like kinase Cdc5 drives exit from pachytene during budding yeast meiosis. *Genes Dev.* **22**, 2627–2632 (2008).
29. P. Jordan *et al.*, Ipl1/Aurora B kinase coordinates synaptonemal complex disassembly with cell cycle progression and crossover formation in budding yeast meiosis. *Genes Dev.* **23**, 2237–2251 (2009).
30. P. W. Jordan, J. Karppinen, M. A. Handel, Polo-like kinase is required for synaptonemal complex disassembly and phosphorylation in mouse spermatocytes. *J. Cell Sci.* **125**, 5061–5072 (2012).
31. A. M. Clemons *et al.*, *akirin* is required for diakinesis bivalent structure and synaptonemal complex disassembly at meiotic prophase I. *Mol. Biol. Cell* **24**, 1053–1067 (2013).
32. B. Argunhan *et al.*, Fundamental cell cycle kinases collaborate to ensure timely destruction of the synaptonemal complex during meiosis. *EMBO J.* **36**, 2488–2509 (2017).
33. T. D. Resnick *et al.*, Mutations in the chromosomal passenger complex and the condensin complex differentially affect synaptonemal complex disassembly and metaphase I configuration in Drosophila female meiosis. *Genetics* **181**, 875–887 (2009).
34. L. Zhaunova, H. Ohkura, M. Breuer, Kdm5/Lid regulates chromosome architecture in meiotic prophase I independently of its histone demethylase activity. *PLoS Genet.* **12**, e1006241 (2016).
35. P. Navarro-Costa *et al.*, Early programming of the oocyte epigenome temporally controls late prophase I transcription and chromatin remodelling. *Nat. Commun.* **7**, 12331 (2016).
36. T. Klymenko *et al.*, A Polycomb group protein complex with sequence-specific DNA-binding and selective methyl-lysine-binding activities. *Genes Dev.* **20**, 1110–1122 (2006).
37. C. Grimm *et al.*, Molecular recognition of histone lysine methylation by the Polycomb group repressor dSfmbt. *EMBO J.* **28**, 1965–1977 (2009).
38. C. Alfieri *et al.*, Structural basis for targeting the chromatin repressor Sfmbt to Polycomb response elements. *Genes Dev.* **27**, 2367–2379 (2013).
39. M. Sarov *et al.*, A genome-wide resource for the analysis of protein localisation in *Drosophila*. *eLife* **5**, e12068 (2016).
40. M. Van Doren, A. L. Williamson, R. Lehmann, Regulation of zygotic gene expression in *Drosophila* primordial germ cells. *Curr. Biol.* **8**, 243–246 (1998).
41. A. H. Brand, N. Perrimon, Targeted gene expression as a means of altering cell fates and generating dominant phenotypes. *Development* **118**, 401–415 (1993).
42. P. Rørth, Gal4 in the *Drosophila* female germline. *Mech. Dev.* **78**, 113–118 (1998).
43. J. Q. Ni *et al.*, A genome-scale shRNA resource for transgenic RNAi in *Drosophila*. *Nat. Methods* **8**, 405–407 (2011).
44. S. E. Hughes *et al.*, The E3 ubiquitin ligase Sina regulates the assembly and disassembly of the synaptonemal complex in *Drosophila* females. *PLoS Genet.* **15**, e1008161 (2019).
45. O. Rog, S. Köhler, A. F. Dernburg, The synaptonemal complex has liquid crystalline properties and spatially regulates meiotic recombination factors. *eLife* **6**, e21455 (2017).
46. F. Frey *et al.*, Molecular basis of PRC1 targeting to Polycomb response elements by PhoRC. *Genes Dev.* **30**, 1116–1127 (2016).
47. H. Kang *et al.*, Sex comb on midleg (Scm) is a functional link between PcG-repressive complexes in *Drosophila*. *Genes Dev.* **29**, 1136–1150 (2015).
48. J. A. Kassis, J. A. Kennison, J. W. Tamkun, Polycomb and Trithorax group genes in *Drosophila*. *Genetics* **206**, 1699–1725 (2017).
49. E. C. Chittock, S. Latwiel, T. C. Miller, C. W. Müller, Molecular architecture of polycomb repressive complexes. *Biochem. Soc. Trans.* **45**, 193–205 (2017).
50. S. Z. DeLuca, M. Ghildiyal, L. Y. Pang, A. C. Spradling, Differentiating *Drosophila* female germ cells initiate Polycomb silencing by regulating PRC2-interacting proteins. *eLife* **9**, e56922 (2020).
51. Z. Durdevic, A. Ephrussi, Germ cell lineage homeostasis in *Drosophila* requires the vasa RNA helicase. *Genetics* **213**, 911–922 (2019).
52. J. Müller *et al.*, Histone methyltransferase activity of a *Drosophila* Polycomb group repressor complex. *Cell* **111**, 197–208 (2002).
53. Y. B. Schwartz *et al.*, Genome-wide analysis of Polycomb targets in *Drosophila melanogaster*. *Nat. Genet.* **38**, 700–705 (2006).
54. A. Birve *et al.*, Su(z)12, a novel *Drosophila* Polycomb group gene that is conserved in vertebrates and plants. *Development* **128**, 3371–3379 (2001).
55. N. Iovino, F. Ciabrelli, G. Cavalli, PRC2 controls *Drosophila* oocyte cell fate by repressing cell cycle genes. *Dev. Cell* **26**, 431–439 (2013).
56. O. S. Rathore *et al.*, NineTeen complex-subunit Salsa is required for efficient splicing of a subset of introns and dorsal-ventral patterning. *RNA* **26**, 1935–1956 (2020).

57. E. Staeva-Vieira, S. Yoo, R. Lehmann, An essential role of DmRad51/SpnA in DNA repair and meiotic checkpoint control. *EMBO J.* **22**, 5863–5874 (2003).
58. M. Klovstad, U. Abdu, T. Schüpbach, Drosophila *brca2* is required for mitotic and meiotic DNA repair and efficient activation of the meiotic recombination checkpoint. *PLoS Genet.* **4**, e31 (2008).
59. J. L. Brown, M. A. Sun, J. A. Kassis, Global changes of H3K27me3 domains and Polycomb group protein distribution in the absence of recruiters Spps or Pho. *Proc. Natl. Acad. Sci. U.S.A.* **115**, E1839–E1848 (2018).
60. H. Kang *et al.*, Variant Polycomb complexes in *Drosophila* consistent with ancient functional diversity. bioRxiv [Preprint] (2022). https://doi.org/10.1101/2022.04.29.490092 (Accessed 1 May 2022).
61. E. Posfai *et al.*, Polycomb function during oogenesis is required for mouse embryonic development. *Genes Dev.* **26**, 920–932 (2012).
62. P. Prudêncio *et al.*, The Trithorax group protein dMLL3/4 instructs the assembly of the zygotic genome at fertilization. *EMBO Rep.* **19**, e45728 (2018).
63. T. Ferreira, P. Prudêncio, R. G. Martinho, *Drosophila* protein kinase N (Pkn) is a negative regulator of actin-myosin activity during oogenesis. *Dev. Biol.* **394**, 277–291 (2014).
64. J. P. Vert, N. Foveau, C. Lajaunie, Y. Vandenbrouck, An accurate and interpretable model for siRNA efficacy prediction. *BMC Bioinformatics* **7**, 520 (2006).
65. S. Kondo, R. Ueda, Highly improved gene targeting by germline-specific Cas9 expression in *Drosophila*. *Genetics* **195**, 715–721 (2013).
66. A. Pereira *et al.*, Coherent-hybrid STED: High contrast sub-diffraction imaging using a bi-vortex depletion beam. *Opt. Express* **27**, 8092–8111 (2019).
67. S. E. Hughes *et al.*, Heterochromatic threads connect oscillating chromosomes during prometaphase I in *Drosophila* oocytes. *PLoS Genet.* **5**, e1000348 (2009).
68. B. Langmead, S. L. Salzberg, Fast gapped-read alignment with Bowtie 2. *Nat. Methods* **9**, 357–359 (2012).
69. P. Danecek *et al.*, Twelve years of SAMtools and BCFtools. *Gigascience* **10**, giab008 (2021).
70. A. Dobin *et al.*, STAR: Ultrafast universal RNA-seq aligner. *Bioinformatics* **29**, 15–21 (2013).
71. Y. Liao, G. K. Smyth, W. Shi, featureCounts: An efficient general purpose program for assigning sequence reads to genomic features. *Bioinformatics* **30**, 923–930 (2014).
72. M. D. Robinson, A. Oshlack, A scaling normalization method for differential expression analysis of RNA-seq data. *Genome Biol.* **11**, R25 (2010).
73. A. T. Lun, Y. Chen, G. K. Smyth, It's DE-licious: A recipe for differential expression analyses of RNA-seq experiments using quasi-likelihood methods in edgeR. *Methods Mol. Biol.* **1418**, 391–416 (2016).
74. M. D. Robinson, D. J. McCarthy, G. K. Smyth, edgeR: A Bioconductor package for differential expression analysis of digital gene expression data. *Bioinformatics* **26**, 139–140 (2010).
75. F. Ramírez *et al.*, deepTools2: A next generation web server for deep-sequencing data analysis. *Nucleic Acids Res.* **44**, W160–W165 (2016).